Digital Keywords

707 Military Derivative Airplane
Aero-Servo-Elastic Flutter Incident
Computer Simulation
CFM56 Engine
E-6 Airplane
EASY5
Fast Fourier Transform (FFT)
Flutter
Frequency Decomposition
NASTRAN Finite Element Model
Power Spectral Density Analysis (PSD)
Robert G. Borst
Rudder Power Control Unit (PCU)
Structural Analysis
TACAMO Mission
Vertical Fin Failure

This is to certify that

Robert G. Borst

is a Winner of the "Best Presentation Award"
for the paper entitled

E-6 Flutter Investigation and Experience

in Session GNC–28 of the 1992
American Institute of Aeronautics and Astronautics
Guidance, Navigation and Control Conference
Hilton Head, South Carolina
August 12-14, 1992

Uy-Loi Ly
1992 GNC Technical Program
Chairperson

P. Douglas Arbuckle
1992 GNC General
Chairperson

David K. Schmidt
GNC TC Chairperson

E-6 Flutter Investigation and Experience

Robert G. Borst* and Robert W. Stromet
Boeing Defense & Space Group, Electronics Systems Division, Air Vehicle Technology
Seattle, Washington

During E-6 airplane flutter testing, two separate incidents occurred which resulted in the partial loss of aircraft vertical tails. In both cases, the aircraft landed without further incident. Linear aero-servo-elastic analyses provided no indication of a flutter instability. Non-linear aero-servo-elastic behavior had to be included to define the instability. Resolution involved gain stabilizing the rudder control system and phase stabilizing the vertical fin structure. Analytical and test results leading to resolution of E-6 aero-servo-elastic flutter are presented. Attention is focused on the multidisciplinary interaction of aerodynamics, flight controls, and structures.

Nomenclature

Constants

A_p = area of PCU piston (8.73 in^2)
b_{fq} = fwd quadrant viscous damp. coeff. (0.8 lbs-sec/in)
b_{aq} = aft quadrant viscous damp. coeff. (0.8 lbs-sec/in)
b_{fc} = feel cam viscous damp. coeff. (4 lbs-sec/in)
b_r = rudder viscous damp. coeff. (17.1 lbs-sec/in)
b_{rt} = upper rudder viscous damp. coeff. (0.31 lbs-sec/in)
b_t = tab viscous damp. coeff. (95.1 lbs-sec/in)
f_{cfq} = fwd quadrant Coulomb friction force (25 lbs)
f_{caq} = aft quadrant Coulomb friction force (10 lbs)
k_c = cable stiffness (375 lbs/in)
k_d = PCU dynamic stiffness (335,000 lbs/in)
k_i = PCU input linkage stiffness (1,200 lbs/in)
k_{fc} = feel cam stiffness (850 lbs/in)
k_{bs} = PCU back-up structure stiffness (580,000 lbs/in)
k_{oil} = PCU oil stiffness (794,000 lbs/in)
k_{rr} = rudder rod stiffness (130,000 lbs/in)
k_s = PCU static stiffness (251,000 lbs/in)
k_{tr} = tab rod stiffness (5,700 lbs/in)
k_{tl} = tab lock stiffness (10,000 lbs/in)
k_{ra} = rudder aerodynamic stiffness (4,200 lbs/deg)
k_{ta} = tab aerodynamic stiffness (170 lbs/deg)
m_{fq} = fwd quadrant mass (0.072 lbs-sec^2/in)
m_{aq} = aft quadrant mass (0.025 lbs-sec^2/in)
m_r = rudder mass (40.32 lbs-sec^2/in)
m_t = tab mass (0.309 lbs-sec^2/in)
P_s = PCU supply pressure (3,000 psi)
P_r = PCU return pressure (50 psi)
R_f = PCU valve/piston followup ratio (0.29)
R_h = PCU valve/housing ratio (0.67)
τ = PCU no-load time constant (0.035 sec)

Variables

δ_r = rudder deflection angle at PCU (deg)
δ_{rt} = rudder deflection angle at upper hinge (deg)
δ_t = rudder tab deflection angle (deg)
f_{aq} = aft quadrant force (lbs)
f_{fc} = feel cam force (lbs)
f_{fq} = forward quadrant force (lbs)
f_r = total force acting on rudder (lbs)
f_{rr} = rudder rod load (lbs)
f_t = total force acting on tab (lbs)
f_{tr} = tab rod load (lbs)
K_l = PCU load factor gain (= 1 unloaded)
K_v = PCU valve flow gain (= 848 in^2/sec unloaded)
Q = PCU measured flow rate (gpm)
Q_p = PCU flow rate (in^3/sec)
θ_{aq} = aft quadrant angle (deg)
θ_{fc} = feel cam angle (deg)
θ_v = PCU valve angle (deg)
x_{aq} = aft quadrant position (in)
x_{fq} = feel cam position (in)
x_h = PCU housing position (in)
x_i = PCU input linkage position (in)
x_p = PCU piston position (in)
x_{tl} = PCU tab lock linkage position (in)
x_v = PCU valve position (in)
S = Laplace operator

Introduction

THE Boeing Company is under contract with the US Navy to develop the E-6 aircraft for TACAMO missions. The E-6, a derivative of the Boeing 707 airframe, is a land-based, subsonic aircraft incorporating modifications necessary to satisfy the Navy mission requirements. The most significant modification is higher thrust CFM56 engines. In order to meet engine failure stability and control requirements during low speed flight, the rudder hydraulic Power Control Unit (PCU) response rate was increased. This increased rate capability adversely affected

Presented as Paper 92-4601 at AIAA Guidance, Navigation, and Control Conference, Hilton Head SC, August 10-12, 1992.
Copyright c 1992 by the American Institute of Aeronautics and Astronautics, Inc. All rights reserved.

*Acting Flight Controls Supervisor. Senior Member, AIAA.

†Lead Structures Engineer. Senior Member, AIAA.

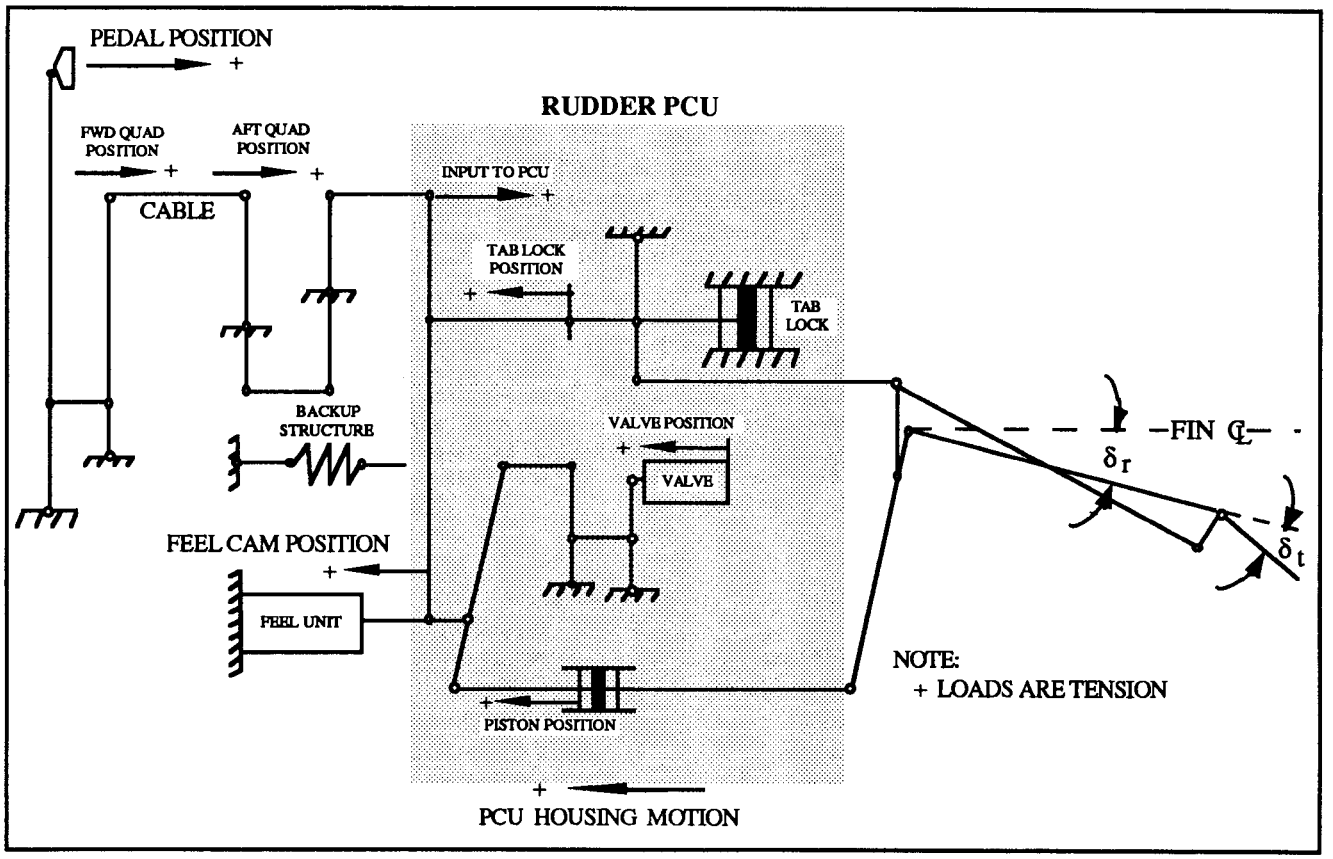

Fig. 1 Schematic of The E-6 Rudder Control System

the E-6 high speed vertical fin flutter characteristics.

During a flutter flight test on February 16, 1989, a divergent dynamic response occurred and the upper third of the vertical fin, part of the rudder, and part of the tab were lost. The aircraft was refurbished, heavily instrumented, and resumed flutter flight testing. On September 28, 1989, a second flutter incident occurred resulting in the upper third of the vertical fin, half of the rudder, and all of the tab being lost. In both cases, the aircraft landed without further incident.

Boeing formed an investigation team and extensive analysis and ground testing were performed from October 1989 through March 1991. Comprehensive aerodynamic, rudder control system, and finite element structural models were developed and independently validated. Finite element structural models were validated by comparison with full scale static and dynamic modal test results. The aerodynamic, control system, and structure models were integrated together to form an aero-servo-elastic model which was correlated against aircraft ground and flight test data. This aero-servo-elastic model was then used to investigate the cause of the instability and evaluate potential aircraft modifications. The aircraft was modified and resumed flutter flight testing on March 4, 1991. The flutter envelop was successfully cleared on April 16, 1991.

This paper provides an overview of analytical and test results leading to E-6 vertical fin flutter resolution. Attention is focused on the multidisciplinary interaction of aerodynamics, flight controls, and structures.

Description of Rudder Control System and Fin Structure

Fig. 1 shows a schematic of the E-6 rudder control system which includes the rudder pedals, forward quadrant, cables, aft quadrant, feel unit, rudder Power Control Unit (PCU), rudder, and tab. Rudder boost pressure is supplied by the auxiliary hydraulic system. The rudder is controlled by conventional rudder pedals, hinged for toe operation of the hydraulic brakes. Movement of the pedals is transmitted by cable and linkage to the valve of the rudder PCU, located in the vertical fin, which deflects the rudder. During powered operation, the tab linkage is hydraulically locked at the rudder PCU and the tab moves in the same direction as the rudder. Artificial feel is provided in proportion to rudder deflection and airspeed. Artificial feel is derived from a spring mechanism wherein the stiffness is modified by a dynamic air pressure linkage (q-bellows).

The E-6 rudder control system also has manual reversion capability. If hydraulic pressure fails or is turned off, the rudder automatically shifts to tab control. The rudder control tab is unlocked and pedal motion operates the control tab to move the rudder assisted by aerodynamic balance panels. In this case, the tab moves opposite to the rudder. Maximum rudder deflection is about one-half and

pedal pressure is double the powered configuration for any given control effect.

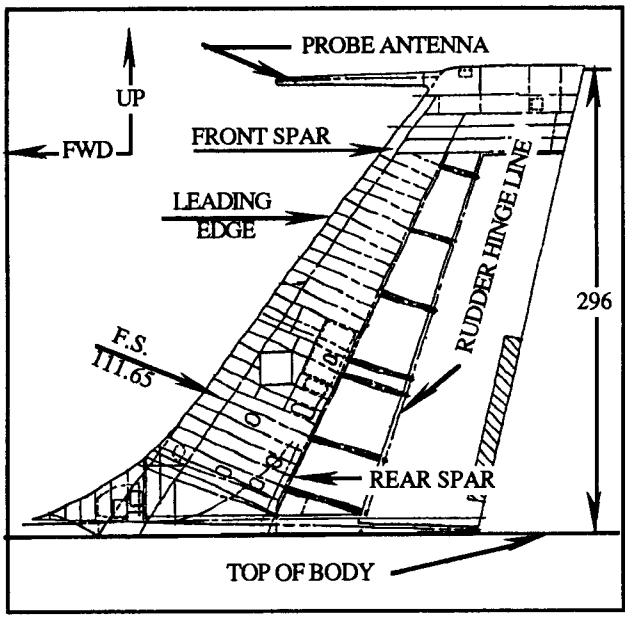

Fig. 2 Fin Structural Layout

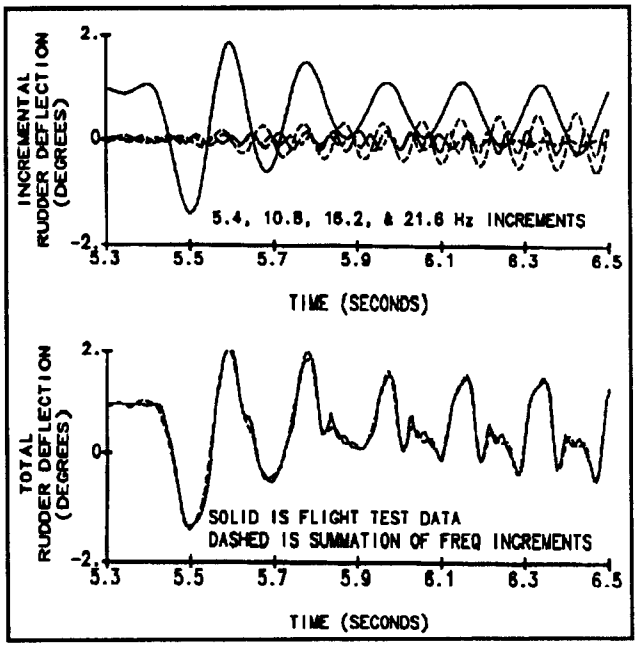

Flg. 3 Frequency Decomposition Of Sept. 28, 1989 Rudder Deflection Angle At PCU

The fin primary structure is a single cell, two spar box of aluminum skin panels supported by ribs running fore and aft between spars. The fin is attached to the fuselage structure by four terminal end fittings. The front spar web is not continuous and ends at Fin Station 111.65 (Fig. 2). Above Fin Station 111.65, the fin box consists of the rear spar web, skin panels, and the leading edge. The leading edge is attached to the box at the front spar chords. The joint at this location has loose tolerance holes so that the leading edge can be easily removed.

September 28, 1989, Flutter Incident Observations

During a developmental flutter flight test on September 28, 1989, the pilot performed a rudder pedal kick with rudder hydraulic boost on at 15,000 feet and 423 KEAS. Approximately three seconds later, the upper third of the vertical fin, half of the rudder, and all of the tab were lost. The airplane landed without further incident. The dominant flutter instability frequency was 5.4 Hertz. It was observed that with rudder boost off, the E-6 was extremely well damped with no tendency toward instability.

A Fast Fourier Transform (FFT) routine[1] was used to calculate the Power Spectral Density (PSD) and hence, frequency content of the September 28, 1989, flight test data. As expected, the largest PSD for the majority of test measurements occurred at 5.4 Hertz. However, the largest PSD for longitudinal PCU support acceleration and longitudinal PCU housing acceleration was 10.8 Hertz. Other PSD peaks occurred at the harmonic frequencies of 16.2 and 21.6 Hertz. Once the frequency content of the data was determined, bandpass filters were designed to breakdown the flight test data into individual frequency components.[2] The bandpass filters used a FFT to convert the time domain flight test data to the frequency domain. The values of the transform within the desired pass band were multiplied by one. The values outside the pass band were multiplied by zero. This modified transform was then converted back to the time domain by the FFT routine. This technique resulted in extremely narrow width bandpass filters with minimal side lobe degradation. The bandpass filter technique was validated by summing the individual frequency components and comparing this summation to the original flight test data. Fig. 3 shows an example of this analysis for the September 28, 1989, flutter incident rudder deflection angle measurement. Fig. 3 also illustrates that superposition of the 5.4 and 10.8 Hertz components was responsible for the one-sided clipping seen in the flight test measurement.

Analyses of the September 28, 1989, incident PCU piston position, rudder deflection angle, and rudder rod load phase relationships provided additional insight. During the flutter instability, the front spar acceleration exhibited the most phase lead. The PCU piston position led the rudder deflection angle, measured at the PCU waterline relative to the fin, by approximately 90 degrees. The rudder deflection angle at the upper hinge waterline was approximately five times larger than the rudder deflection angle at the PCU waterline and exhibited 70 degrees of phase lag. The rudder rod load and rudder deflection angle were initially in phase, but then transitioned to a 180 degree out of phase condition.

Rudder Control System Analyses

Two analysis formulations of the rudder control system shown in Fig. 1 were developed. A linear transfer function representation was used for frequency domain flutter analyses and time domain simulation. A non-linear physical representation was used for time domain simulation and experimentation.[3] Both rudder control system formulations were validated by back driving the models with test measured rudder pedal force, rudder rod load, and tab rod load. There was good agreement between analysis model displacements and test measured displacements. The rudder control system physical formulation is described in detail in the integrated aero-servo-elastic flutter model section of this paper.

The combined rudder control system elements forward of the PCU exhibited a second order system response characteristic. The natural frequency varied from approximately 3 Hertz to 6 Hertz as dynamic pressure increased. The damping ratio varied from approximately 0.2 to 0.05 as dynamic pressure increased. The rudder control system natural frequency and damping ratio during the September 28, 1989, flutter incident flight condition were approximately 5.4 Hertz and 0.07, respectively. It can be shown[4] that the E-6 rudder PCU input to output displacement transfer function behaves like the following first order lag:

$$\frac{x_p}{x_i} = \frac{1.31}{[\tau S+1]} \tag{1}$$

where:

$$\tau = \frac{A_p}{R_f k_v} \tag{2}$$

The 10.8 Hertz frequency component observed in the September 28, 1989, flutter incident data is the result of two separate frequency doubling mechanisms: yaw rotation of the PCU housing and PCU dual concentric valve design. The PCU, which is mounted on back-up structure offset from the fin center line, rotates two cycles for every cycle of rudder deflection. The PCU dual concentric valve design characteristics cause the flow rate (and differential pressure across the PCU piston) to change direction twice for every cycle of rudder deflection. The low amplitude 16.2 and 21.6 Hertz frequency components, also observed in the flutter incident data, result from harmonic frequency summation of the 5.4 and 10.8 Hertz components. The break frequency ($1/2\pi\tau$) of the E-6 PCU, represented by the Eq. (1) first order lag, is approximately 4.5 Hertz. Consequently, there is significant attenuation of frequency components greater than 5.4 Hertz from a PCU input to output displacement transfer function perspective. These high frequency components, however, are directly transmitted to the rudder via the PCU housing structure path.

The flutter speed of an aircraft aerodynamic surface is greatly affected by the structure torsional stiffness. The rudder PCU installation stiffness represents a significant portion of this overall torsional stiffness. It can be shown[4] that the rudder PCU installation behaves like the following complex spring as seen by an external force generator or load:

$$\frac{f_{rr}}{x_p} = \frac{k_s [\tau S + 1]}{\left[\frac{\tau k_s S}{k_d} + 1\right]} \tag{3}$$

where:

$$k_s = \frac{R_f k_{bs}}{R_h} \tag{4}$$

$$k_d = \frac{k_{bs} k_{oil}}{[k_{bs} + k_{oil}]} \tag{5}$$

In order for the PCU installation to be stable, the phase angle of the complex spring shown in Eq. (3) must be positive (i.e., x_p lags f_{rr}). Physically, this means that the force generator is supplying energy which is dissipated by the complex spring. A PCU having this characteristic will provide additional damping. In addition, it can be shown that in the absence of external damping, the low frequency or static stiffness (Eq. 4.) must be less than the high frequency or dynamic stiffness (Eq. 5.) presented to the load for a given installation to be stable. In order to maximize flutter margin and also ensure PCU installation stability, the conventional philosophy is to design the stiffest system possible while maintaining this static and dynamic stiffness relationship.

It is interesting to compare E-6 and 707 PCU installation stability. The E-6 and 707 PCU installations have the same dynamic stiffness (335,000 lbs/in) by virtue of sharing the same back-up structure and PCU oil stiffness. However, the E-6 and 707 PCU linkage ratios are quite different. R_f values for E-6 and 707 PCU installations are 0.29 and 0.95, respectively. Assuming a fixed PCU input linkage, R_h values for E-6 and 707 PCU installations are 0.67 and 2.19, respectively. As a result, the E-6 and 707 PCU installations have the same R_f / R_h ratio (0.43), and hence the same static stiffness (251,000 lbs/in). Consequently, both PCU installations are stable and exhibit identical stability margin. This is consistent with historical experience; both PCU installations have never exhibited instability on the ground or in flight. Note, however, that equal stability margin does not imply equal closed-loop transient response characteristics.

During E-6 powered operation, 3000 psi hydraulic supply pressure is available to the rudder PCU. For the E-6 rudder PCU, this equates to a no-load rudder rate of 64 deg/sec. The maximum differential pressure across the E-6 PCU piston is limited in two airspeed steps in order to prevent loads, due to rudder deflection, from exceeding

structural limits. Between 175 and 250 KIAS, the PCU piston differential pressure limit is set to 2250 psi. Above 250 KIAS, the PCU piston differential pressure limit is set to 1450 psi. An override switch can be used at any airspeed to restore the available piston differential pressure to full system supply pressure. Limiting PCU differential pressure has the effect of decreasing maximum available rudder angle without decreasing rudder rate capability.

In contrast, the 707 no-load rudder rate is 51 deg/sec at 3000 psi supply pressure. The 707 PCU supply pressure is reduced to 2250 psi above 250 KIAS. Reducing PCU supply pressure to 2250 psi has the effect of decreasing the maximum available rudder angle and decreasing the rudder rate capability to 44 deg/sec. Fig. 4 shows rudder rate as a function of opposing rudder rod load and illustrates the significant rate capability difference between E-6 and 707 aircraft.

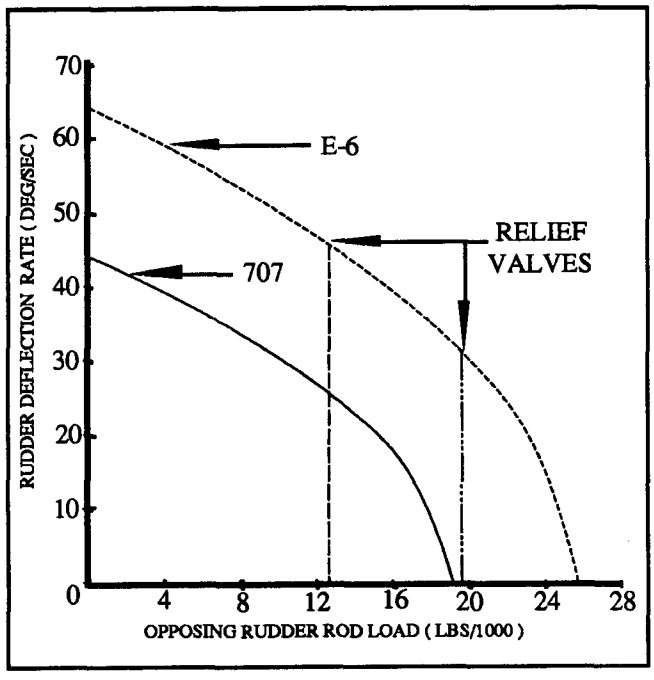

Fig. 4 E-6 & 707 Rudder Rate Characteristics

Rudder Control System Laboratory Test Results

The laboratory test article was a newly completed production vertical tail assembly. The fin assembly was mounted vertically to a rigid steel I-beam test fixture. The assembly included all structural elements, all control system components, and all avionic systems. Forward rudder control system elements were simulated with a mass, spring, and damper setup tuned to the control system natural frequency and damping. Inputs to the control system were applied with a calibrated hammer impact mechanism to simulate a rudder pedal kick. The objective was to validate control system analyses, measure structural interaction effects, and obtain data for a non-linear control system analysis model.

Results of hammer impact tests showed control system damping decreased as hydraulic pressure increased, as input pedal kick energy increased, and as the feel unit dynamic air pressure (q-bellows) increased. Sinusoidal forces were applied to the rudder control system input, rudder, and tab to determine system transfer functions. There was good agreement between rudder control system analysis predictions and laboratory test data.

During hammer impact testing, it was observed that the rudder rod load was always 180 degrees out of phase with the rudder deflection angle. This is what is expected when stiff, lightly damped structure is driven at a frequency below its natural frequency. It was also observed that control system damping was significantly less on the ground than normally seen in flight. The test was repeated with the rudder and tab removed, thereby eliminating the rudder rod and tab rod loads. Control system damping was significantly increased. This test demonstrated that the lightly damped control system response was due to PCU housing position feedback into the rudder control system. The PCU housing position feedback was proportional to rudder rod load resulting from dynamic excitation of the rudder and fin structure with inherently low structural damping. In flight, in the presence of aerodynamics, damping is significantly increased and the rudder rod load and rudder deflection angle are normally in phase.

Prior to the resumption of flight testing, the E-6 hydraulic system was modified to decrease the no-load rudder rate to levels similar to the 707 airplane (44 deg/sec). A pressure reducer was installed to limit the PCU supply pressure to 2250 psi. At 2250 psi supply pressure, the E-6 rudder rate was 55 deg/sec. A flow restrictor was installed to further reduce rudder rate. The net effect of both these modifications was to decrease the E-6 no-load rudder rate capability to 35 deg/sec.

As a final precaution, a hydraulic dump system was designed and tested. The hydraulic dump system was proposed as an in-flight "safety net" for the verification flutter test only. The purpose of the hydraulic dump system was to remove the energy input to the fin by the rudder PCU in the event a flutter divergence were to occur. This was accomplished by dumping the hydraulic pressure to the PCU whenever sensed fin tip lateral acceleration became large (greater than 15 g's) or divergent (second positive occurrence of pilot selected 5, 8, or 12 g threshold).

Structures Analysis

In order to obtain an accurate stiffness representation of the vertical fin for aero-servo-elastic flutter analysis, detailed finite element models of the fin and aft fuselage were built using the NASTRAN Finite Element Code.[5,6] The fin finite element model consisted of 2500 grids (14,000 degrees of freedom) and 12,600 elements (Fig. 5). The aft fuselage model had 700 grids and 4000 degrees of freedom. The fin model was validated by comparison with full-scale static and dynamic (modal) vertical fin test data.

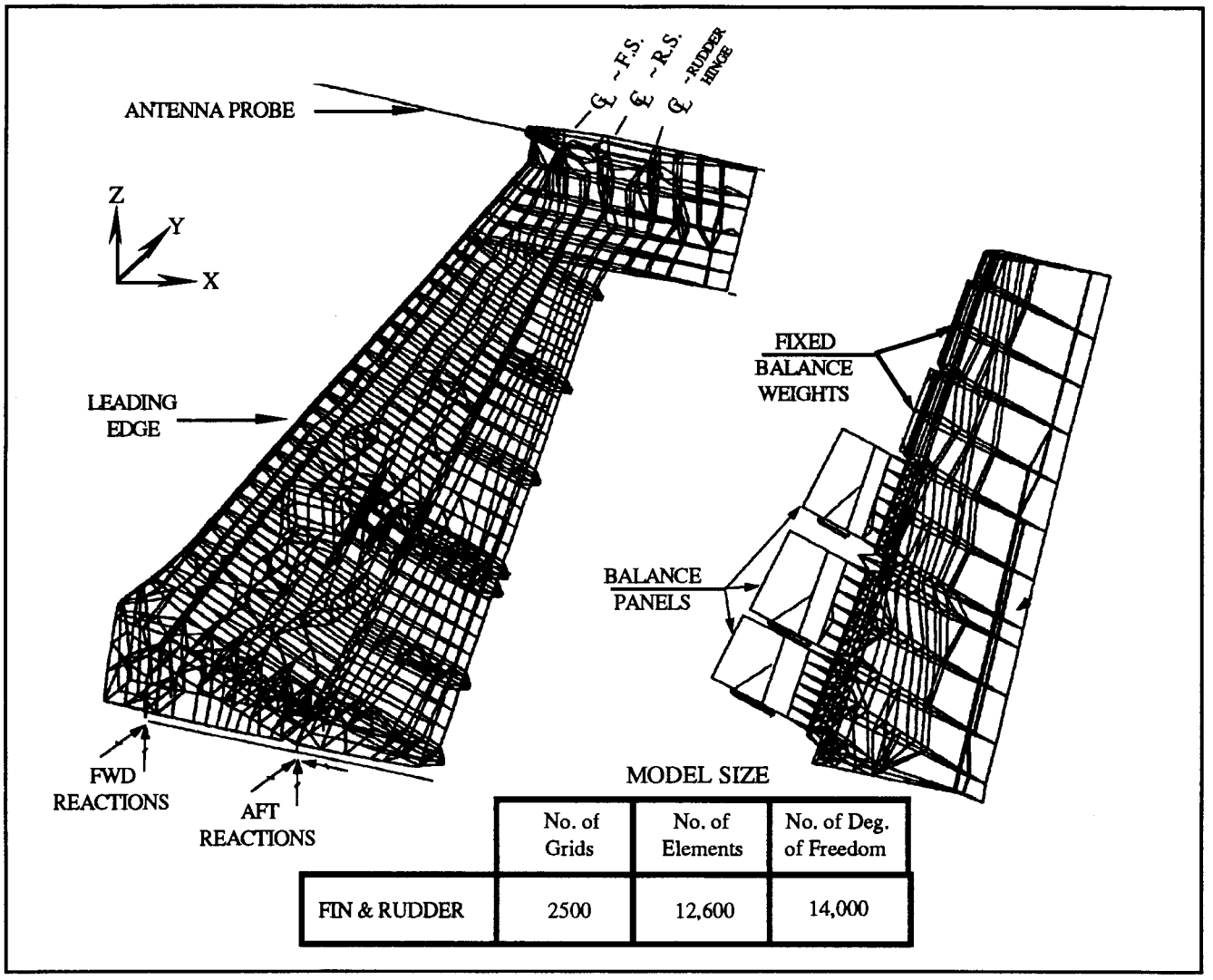

	No. of Grids	No. of Elements	No. of Deg. of Freedom
FIN & RUDDER	2500	12,600	14,000

Fig. 5 E-6 Vertical Fin Nastran Finite Element Model

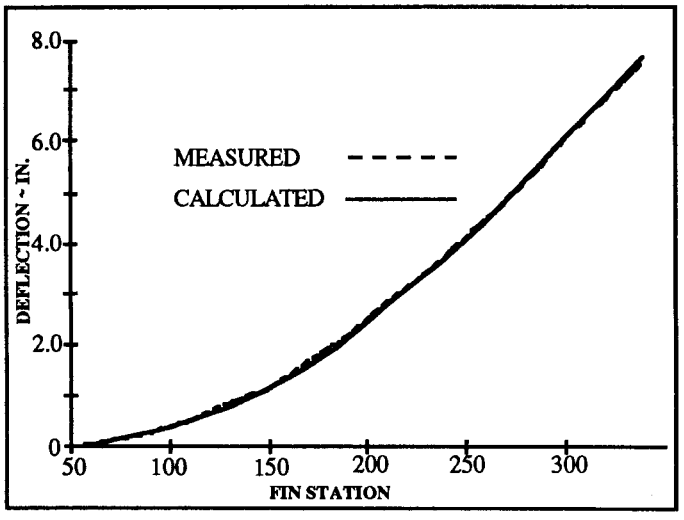

Fig.6 Fin Static Deflection

A comparison between calculated and measured static deformation for a bending loadcase is shown in Fig. 6. Excellent correlation was obtained. Good correlation was also obtained with the other test loadcases (torsion and combined bending and torsion).

Comparisons between calculated and measured modal data are shown in Fig. 7. Modal deformations were measured at 165 locations on the fin. Calculated modal deformations were extracted from the NASTRAN model output at these same points for the first ten modes, resulting in a 165x10 matrix of analysis mode shapes. The calculated mode shapes were evaluated by performing a cross-orthogonality calculation consisting of the matrix triple product:

$$[\text{Ortho}] = [\phi^{\text{Test,GM}}]^T [M] [\phi^{\text{Anal,GM}}] \qquad (6)$$

where:

[Ortho] = orthogonality matrix (10x10 for 10 mode shapes)

$[\phi^{Test,GM}]$ = test mode shape matrix normalized to unit generalized mass (165x10).

[M] = analytic mass matrix at test locations (165x165).

$[\phi^{Anal,GM}]$ = analysis mode shape matrix normalized to unit generalized mass (165x10).

$[\phi]^T$ = transpose of mode shapes

$$\{GM\}_{Mode\ i} = \{\phi^{Test}\}^T_{Mode\ i}\,[M]\,\{\phi^{Test}\}_{Mode\ i} \quad (7)$$

$$\{\phi^{Test,GM}\}_{Mode\ i} = \frac{\{\phi^{Test}\}_{Mode\ i}}{\sqrt{\{GM\}_{Mode\ i}}} \quad (8)$$

$$\{\phi^{Anal,GM}\}_{Mode\ i} = \frac{\{\phi^{Anal}\}_{Mode\ i}}{\sqrt{\{GM\}_{Mode\ i}}} \quad (9)$$

The mass matrix used in this calculation was obtained by performing a Guyan reduction[7] to 165 degrees of freedom at the test measurement points, resulting in a 165x165 mass matrix. A value of from 0.90 to 1.0 for a diagonal term of the orthogonality matrix combined with low values for off-diagonal terms (< 0.15 to 0.20) indicated close correlation between test and analysis mode shapes. Excellent correlation was obtained for the first eight mode shapes and frequencies.

Structure Static and Dynamic Laboratory Test Results

Full-scale static and dynamic testing were conducted to evaluate the fin structural behavior and validate the fin finite element model. An area of interest was the post-buckling behavior of the fin. It was known that the fin skins buckled at relatively low loads. Although analyses showed that buckling had a relatively small effect on fin torsional stiffness (approximately 10%), verification by test was desired since aircraft flutter speed is greatly affected by torsional stiffness. During both tests the fin was cantilevered off the base at the terminal end fitting locations. Loads were applied by hydraulic actuators mounted off a strongback. Static loads consisted of three primary load cases: torsion, bending, and a combination of both which simulated estimated fin loads during the second flutter incident.

Structural behavior was as predicted by finite element and hand analysis except the fin exhibited non-linear behavior under certain loading conditions. When the applied torsion exceeded a certain level, fin twisting deformations increased dramatically (Fig 8). It was found that this occurred when the shear across the leading edge joint exceeded a certain level. Further investigation determined that this was not caused by buckling, but rather by slippage between the leading edge fairing and the front spar chords

Fig. 7 E-6 Fin ~ Comparison Of Test And Analysis Modes Low Level (Fin With And Without Web Extension)

MODE DESCRIPTION (LOW LEVEL DATA)		TEST FREQ. (cps)	ANALYSIS FREQ. (cps)		FREQUENCY (Analysis/Test)		CROSS ORTHOGONALITY [2]	[2]	[3]
	Mode #	No Web [1]	No Web	w/Web	No Web	w/Web	No Web	w/Web	w/ or w/o Web
First Fin Y Bending	1	4.63	4.69	4.68	1.01	1.01	1.00	1.00	0.07
Rudder Rotation	2	7.08	7.10	7.10	1.00	1.00	0.94	0.94	0.08
Second Fin Y Bndg. (w/Aero-Balance Panels)	3	11.02	11.36	11.36	1.03	1.03	0.95	0.95	0.15
Fin Chordwise Pitching	4	13.63	14.00	14.04	1.03	1.03	0.99	0.99	0.07
Fin Tip Twist	5	14.77	15.54	15.59	1.05	1.05	0.96	0.96	0.08 [4]
Fixed Balance Weights w/Fin Bndg. + Tip Twist	6	15.35	14.97	14.99	0.98	0.98	0.90	0.90	0.17
Probe Antenna Vertical	7	19.86	19.05	19.05	0.96	0.96	1.00	1.00	0.02
Fin Torsion	8	21.86	22.85	22.75	1.05	1.05	0.92	0.94	0.14
Third Fin Bending + Rudder Twist	9	23.44	23.25	23.24	0.99	0.99	0.80	0.80	0.39
Rudder Twist + Tip Twist	10	25.72	25.59	25.63	0.99	0.99	0.83	0.83	0.51

[1] Test modes and frequencies with web were not used since results were distorted by loose probe joint.

[2] Diagonal term of [ORTHO] , Eq. (6)

[3] Largest off-diagonal term

[4] A higher value of 0.38 was obtained between analysis mode 5 and test mode 6.

which occurred when the frictional forces due to fastener preload were overcome. Slippage occurred until the gaps between the fasteners and the edges of the holes were closed. The leading edge joint detail is shown in Fig. 9. During repeated loadings in the same direction, the slip effect was reduced since the fasteners were already bearing on the edge of the holes. The slip behavior was found to be repeatable after removing and replacing the leading edge.

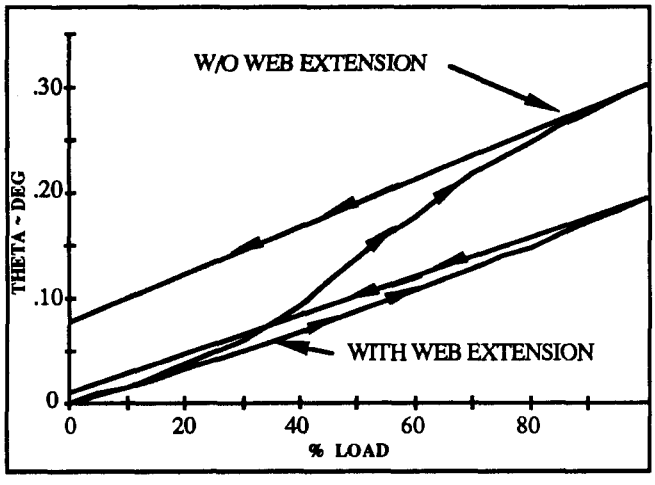

Fig. 8 Fin Torsional Deflection vs. Load (Twist Over 18in. Panel)

Dynamic (modal) testing of the fin initially did not show a pronounced slip behavior. Test amplitudes were not sufficient to exceed the preload in the leading edge fasteners. During subsequent testing, the leading edge fasteners were loosened in order to observe the effect of slip on fin modes and frequencies. Frequencies for torsional modes were significantly reduced by leading edge slip. The tip twist modal frequency decreased by 34% and the torsion modal frequency decreased by 18%. Fig. 10 shows the effect of slip on the tip twist frequency versus force input to the fin. Frequency decreased with increasing force input but eventually leveled off as the slip limit was reached.

As a result of test and analysis, which showed the slip mechanism to be a possible contributor to fin flutter, a front spar web was added above Fin Station 111.65 to ensure that fin torsional stiffness would be maintained without relying on leading edge fairing friction for shear flow transmission. Subsequent static and dynamic testing with the web extension installed confirmed that this design change maintained torsional stiffness and prevented slip. Static test results are shown in Fig. 8. Dynamic test results for the tip twist mode are shown in Fig. 10. When the leading edge was loosened, with the web extension installed, there was negligible change in frequency.

The apparent tip twist frequency decrease of 8-10%, with the web extension installed (Fig. 10), was determined to be due to degradation of the stiffness of the antenna probe base support in the fin tip. Inspection and testing showed that the fiberglass probe base had been damaged by dynamic testing of the fin. This occurred between the time when the original dynamic test was run and when the test was re-run with the web extension installed. This degradation was attributed to the large number of cycles applied to the fin during this interim period. This environment was much more severe than would ever be encountered in actual service. This data along with the finite element analysis gave confidence that the web extension would prevent slip and improve flutter characteristics.

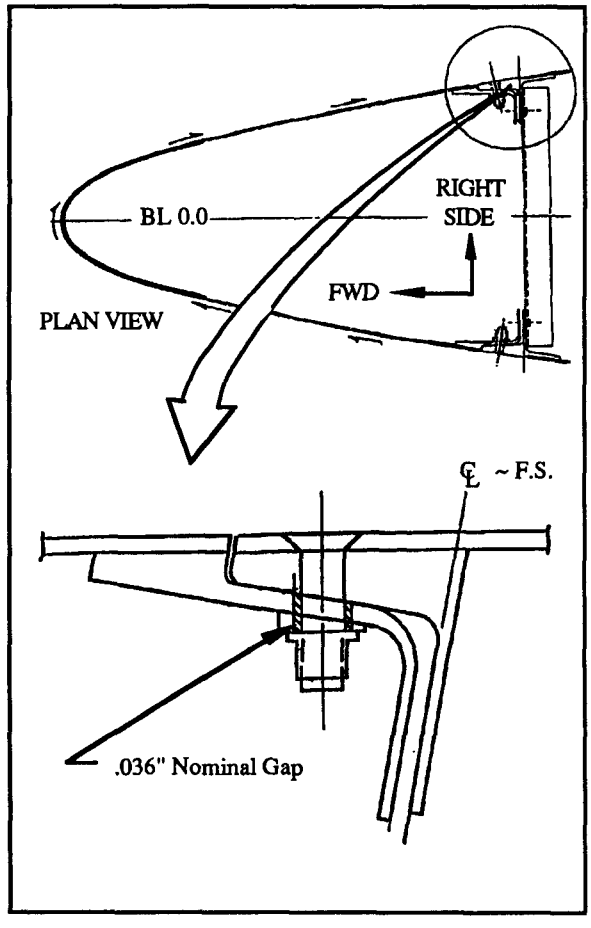

Fig. 9 Vertical Stabilizer Leading Edge Installation

During the September 28, 1989, flutter incident, the rudder deflection angle at the upper hinge was approximately five times larger than the rudder deflection angle at the PCU (both deflections measured relative to fin structure) and exhibited 70 degrees of phase lag. This difference in relative displacement was not due to rudder twist since the rudder was determined to be relatively stiff, but was due to increased fin tip twist resulting from leading edge slip.

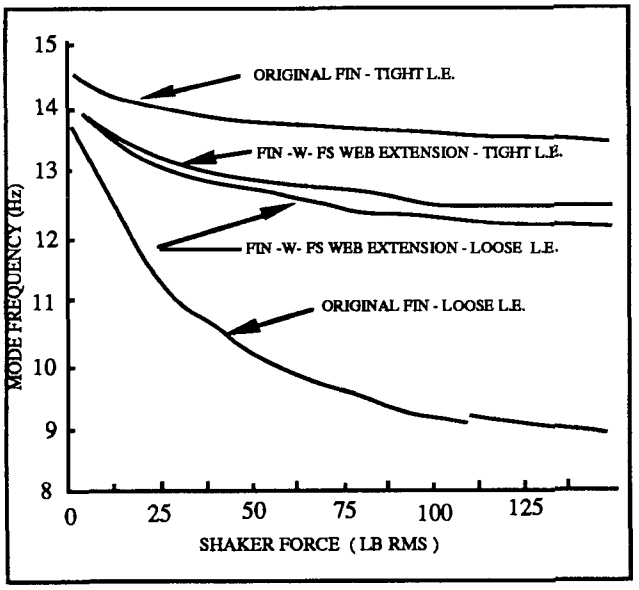

Fig. 10 Tip Twist Mode Frequency vs. Input Force

Integrated Aero-Servo-Elastic Flutter Model

The validated NASTRAN model of the vertical fin was reduced to approximately 250 degrees of freedom for use in aero-servo-elastic flutter analyses. This model was merged with another NASTRAN model of Section 48 (Fig. 11) and a "stick" model representation of the remaining airplane. The models were merged using component mode

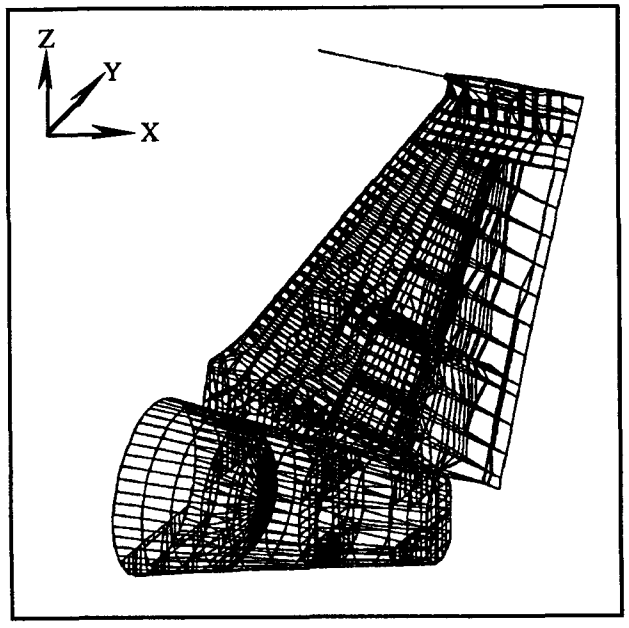

Fig. 11 Nastran Fin, Rudder, And Section 48 FEM Model

synthesis techniques. Degrees of freedom were provided in the fin model to permit merging of the rudder control system. Linear aero-servo-elastic flutter analyses performed with this model correlated fairly well with ground test and benign flight test conditions. Linear aero-servo-elastic analyses, however, provided no indication of flutter instability and, in fact, predicted substantial flutter margin (100-200 KIAS).

Fortunately, the aforementioned analyses and testing quantified key system parameters and provided sufficient knowledge of non-linear behavior to permit an empirical understanding of the phenomena responsible for E-6 flutter instability. Control system and structural non-linearities are difficult to model exactly. Further, the problem becomes compounded when these non-linearities interact. The challenge was to validate an empirical model to permit definition of a design change that would ensure stability.

A simplified aero-servo-elastic flutter analysis model based on a physical representation of the rudder control system is presented to facilitate discussion and illustrate the mechanisms responsible for E-6 vertical fin flutter. The only input to the analysis model is the rudder pedal force test measurement. All numbers shown in the following equations represent kinematic linkage ratios. Several redundant variables are calculated to permit direct comparison with test data. Standard simulation techniques and practices were used.[8,9]

Forward and aft quadrant forces (f_{fq} and f_{aq}) are calculated as follows:

$$f_{fq} = 0.808\, f_{pedal} - k_c\,[x_{fq} - x_{aq}] \qquad (10)$$

$$f_{aq} = k_c[x_{fq} - x_{aq}] - 0.624\, k_i\,[0.624\, x_{aq} - x_i] \qquad (11)$$

Forward quadrant, aft quadrant, and PCU input linkage displacements (x_{fq}, x_{aq}, and x_i) are calculated as follows:

$$x_{fq} = \frac{[f_{fq} - b_{fq}\, x_{fq}\, S - \text{Sign}\,(x_{fq}S)\, f_{cfq}]}{[m_{fq}\, S^2]} \qquad (12)$$

$$x_{aq} = \frac{[f_{aq} - b_{aq}\, x_{aq}\, S - \text{Sign}\,(x_{aq}S)\, f_{caq}]}{[m_{aq}\, S^2]} \qquad (13)$$

$$x_i = \frac{[2.1\, k_i\, x_{aq} - 0.624\, b_{fc}\, x_{fc}\, S]}{[3.36\, k_i + 2.1\, k_{fc}]} \qquad (14)$$

Aft quadrant and feel cam angles (θ_{aq} and θ_{fc}) are calculated as follows:

$$\theta_{aq} = 8.01\, x_{aq} - 29.2\,[x_h + x_{tl}] \qquad (15)$$

$$\theta_{fc} = 11.3\, x_i + 19.7\,[x_h + x_{tl}] \qquad (16)$$

Note the PCU housing position and tab lock position feedback paths. PCU housing position feedback is included in the PCU installation design as shown by Eq. (3). The tab lock position feedback, however, results from having a manual reversion system. When rudder and tab loads are out of phase, as they were during the September 28, 1989 incident, the tab lock feedback negates the PCU housing

feedback and is destabilizing. It is important that PCU supply pressure be maintained sufficiently high to prevent the tab lock from unlocking during powered operation.

PCU valve position and angle (x_v and θ_v) are calculated as follows:

$$x_v = 0.0341\ \theta_{fc} - 0.293\ x_p \tag{17}$$

$$\theta_v = 91.7\ x_v \tag{18}$$

Note that the PCU housing position feedback creates valve motion opposite to that caused by the PCU piston position followup feedback. The PCU housing position feedback tends to reduce the stiffness of the PCU installation at low frequency as shown by Eq. (4) and prevents instability as illustrated by Eq. (3).

PCU load factor, flow rate, valve flow gain, measured flow rate, and piston position (K_l, Q_p, K_v, Q, and x_p) are calculated as follows:

$$K_l = \frac{\left[P_s - P_r - \frac{\text{Sign}\,(x_v)\, f_{rr}}{A_p}\right]}{[P_s - P_r]} \tag{19}$$

Q_{nl} = bench test flow rate data versus x_v

$$Q_p = Q_{nl}\sqrt{K_l} \tag{20}$$

$$K_v = \frac{Q_p}{x_v} \tag{21}$$

$$Q = 0.260\ |Q_p| \tag{22}$$

$$x_p = \frac{K_v\, x_v}{A_p\, S} - \frac{f_{rr}}{k_{oil}} \tag{23}$$

The inclusion of non-linear PCU flow rate characteristics, as shown by Eq. (19) and Eq. (20), are necessary to induce instability in the analysis model and achieve test data and analysis model correlation. Eq. (19) and Eq. (20) take into account the rudder rod load effect on PCU flow rate. Note that opposing loads reduce the effective PCU flow rate gain (Eq. 21) while assisting loads increase the effective rate gain. This allows the aero-elastic loads to interact with the control system. The PCU flow rate gain varied ±20% from its no-load value during the September 28, 1989, incident. Adding the PCU supply pressure reducer and flow restrictor modifications reduced the PCU rate capability by 55% and effectively gain stabilized the E-6 aero-servo-elastic flutter system.

Rudder rod load and tab rod load (f_{rr} and f_{tr}) are calculated as follows:

$$f_{rr} = -\,k_{rr}\left[\frac{\delta_r}{12.7} - x_p - x_h\right] \tag{24}$$

$$f_{tr} = -\,k_{tr}\left[\frac{\delta_t}{27.6} - \frac{0.78\ \delta_r}{27.6} - 1.92\ x_{tl} - x_h\right] \tag{25}$$

Total forces on rudder and tab (f_r and f_t) are calculated as follows:

$$f_r = f_{rr} - \frac{k_{ra}\,[3\delta_r + \delta_{rt}]}{4} \tag{26}$$

$$f_t = f_{tr} - k_{ta}\,\delta_t \tag{27}$$

Note that the aerodynamic force acting on the rudder is made proportional to the weighted average of the rudder deflection angle at the PCU and the rudder deflection angle at the upper hinge as shown by Eq. (26). This allows the non-linear structural behavior to interact with the aerodynamics. Use of static aerodynamic theory, which does not account for aerodynamic compressibility or lag effects, was validated by comparison with linear analysis results, that included lifting surface unsteady aerodynamics.

PCU housing and tab lock positions (x_h and x_{tl}) are calculated as follows:

$$x_h = -\,\frac{f_{rr}}{k_{bs}} \tag{28}$$

$$x_{tl} = -\,\frac{0.521\ f_{tr}}{k_{tl}} - \frac{0.00516\ k_{fc}\ \theta_{fc}}{k_{tl}} \tag{29}$$

Tab deflection angle and rudder deflection angle at the PCU (δ_t and δ_r) are calculated as follows:

$$\delta_t = \frac{27.6 f_t}{[m_t\,(S^2 + b_t\,S)]} \tag{30}$$

$$\delta_r = \frac{12.7\ f_r}{[m_r\,(S^2 + b_r\,S)]} \tag{31}$$

Rudder deflection angle at the upper hinge (δ_{rt})is calculated as follows:

$$\delta_{rt} = \delta_r, \text{ or} \tag{32}$$

$$= \frac{3500\delta_r}{[S^2 + b_{rt}\,S + 986]} \tag{33}$$

depending on the state of non-linear fin structure.

It is necessary to include the effect of non-linear fin structure leading edge slip behavior in order to induce instability in the analysis model. The Eq. (33) transfer function calculates the upper rudder hinge deflection angle relative to fin structure with an approximation of the effect of fin leading edge slip. The intent of Eq. (33) is to introduce 70 degrees of phase lag between the two rudder deflection angles as observed during the September 28, 1989 incident. Fig. 12 shows the results of this approximation;

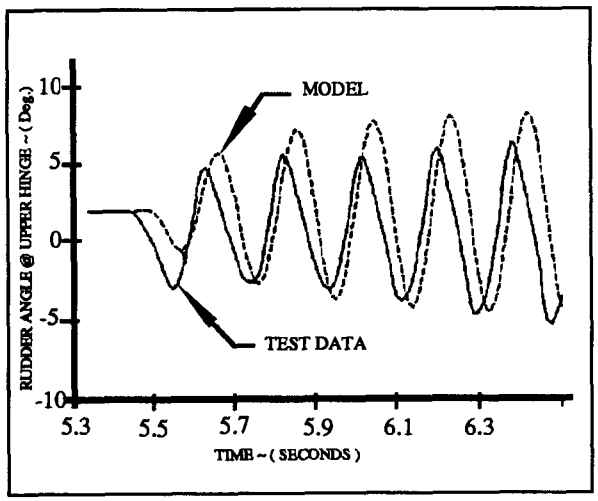

Fig. 12 Approximation Of Effect Of Non - Linear Structure On Rudder Angle @ Upper Hinge

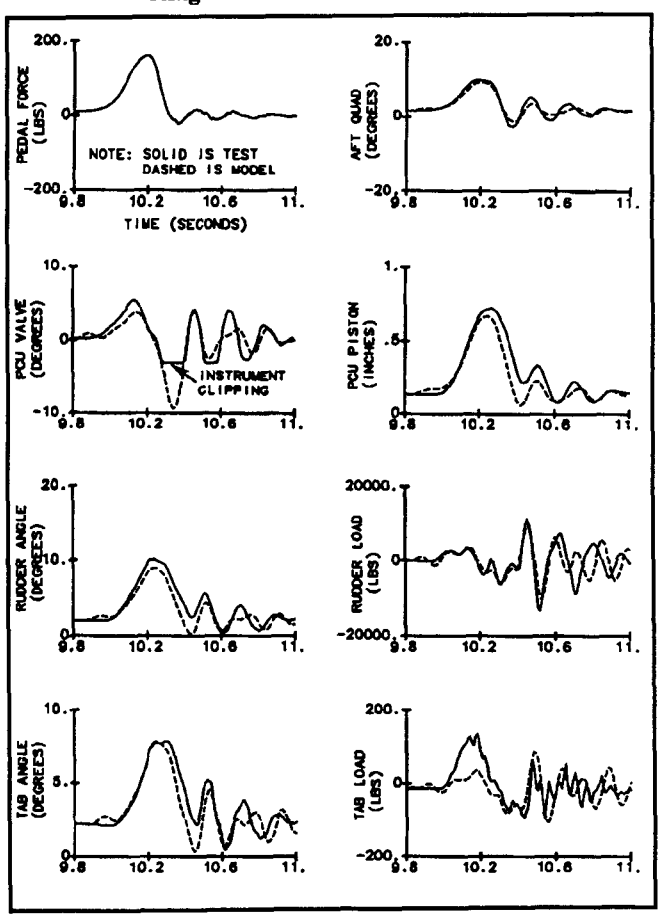

Fig. 13 Servo - Elastic Model Correlation With Ground Test Data

the September 28, 1989, flutter incident upper hinge rudder deflection angle is compared with the Eq. (33) result. Eliminating fin leading edge slip effectively phase stabilized the E-6 aero-servo-elastic flutter system.

Fig. 13 shows ground test data and simplified servo-elastic analysis model correlation. Note that the rudder rod load is always 180 degrees out of phase with the rudder deflection angle. The analysis model is significantly less damped with the rudder and tab aerodynamic stiffness terms set to zero. The analysis model damping increases significantly if the rudder and tab mass terms are then set to zero (i.e., rudder and tab removed). This agrees with previous rudder control system analyses and laboratory test results.

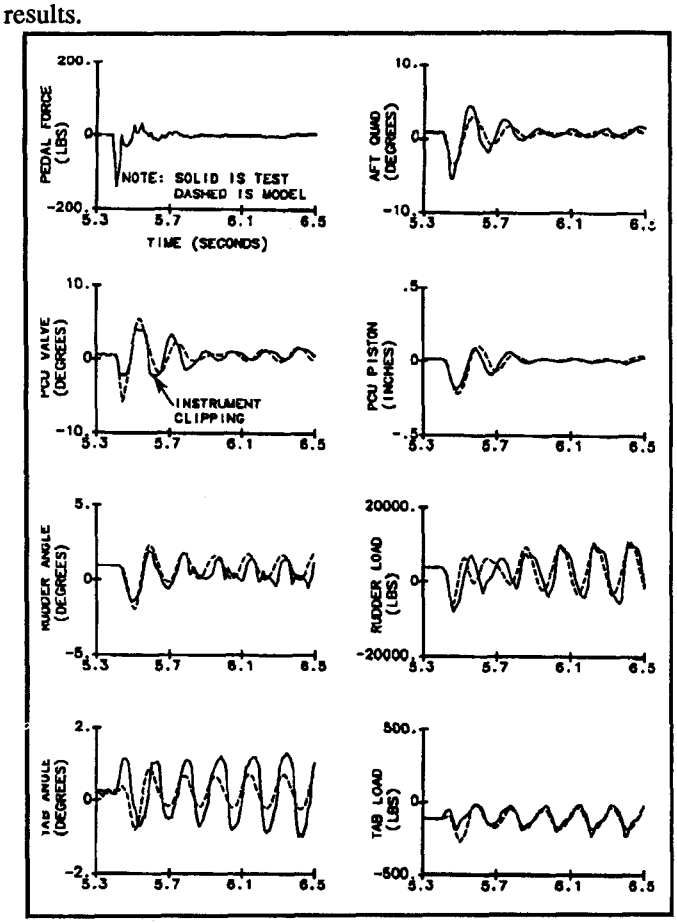

Fig. 14 Aero - Servo - Elastic Flutter Model Correlation to Sept. 28, 1989 Flutter Incident Data

Fig. 14 shows the September 28, 1989, flutter incident flight test data and simplified aero-servo-elastic flutter analysis model correlation. Note that the rudder rod load and rudder deflection angle are initially in phase and then transition to a 180 degree out of phase condition.

E-6 Airplane Ground and Flight Test Results

Airplane ground tests were performed to verify that rudder control system performance, as modified and installed in the airplane, agreed with analyses and laboratory test predictions. Critical control system elements were cooled with vaporized liquid nitrogen to simulate high altitude temperature extremes. The modified rudder control system functioned as expected. An airworthiness review was conducted and the E-6 was ready to resume flutter flight testing.

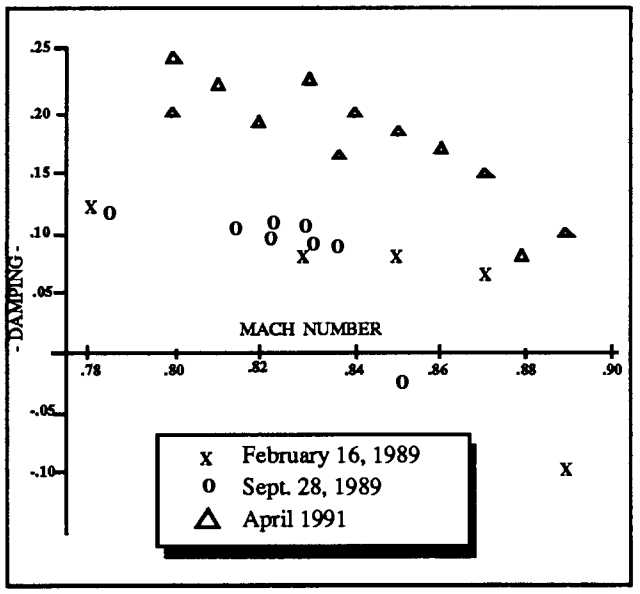

Fig. 15 E-6 Fin Damping @ 15,000 ft.

The flutter flight test program was conducted in four distinct airspeed phases to minimize risk as the flight envelop was expanded. Rudder control system modifications were evaluated during initial flutter flight test phases. Sufficient time was provided between successive phases to permit detailed flight test data analyses. The final rudder control system configuration was selected prior to the last flutter flight test phase and included the PCU supply pressure reducer and flow rate restrictor. The final flutter flight test confirmed adequate damping at critical airspeeds and altitudes as shown in Fig. 15. Fig. 16 shows the successful April 16, 1991, flutter test data and simplified aero-servo-elastic flutter analysis model correlation with final modifications included .

The production rudder control system modifications are automatically switched into the hydraulic system at airspeeds above 250 KIAS. Annunciation is provided to warn the pilot if these modifications fail to operate as designed. An override switch is provided to restore PCU supply pressure to 3000 psi and bypass the PCU flow rate restrictor if required by the pilot. Stability and control flight tests were performed and handling qualities were demonstrated to be adequate with the production rudder control system modifications.

Conclusions

E-6 vertical fin flutter instability was attributable to interacting non-linear behavior present in the rudder control system and fin structure. The original E-6 rudder control system design, which significantly increased the rudder PCU rate capability relative to the historically flutter free 707 design, magnified the effect of these interactions and caused flutter instability.

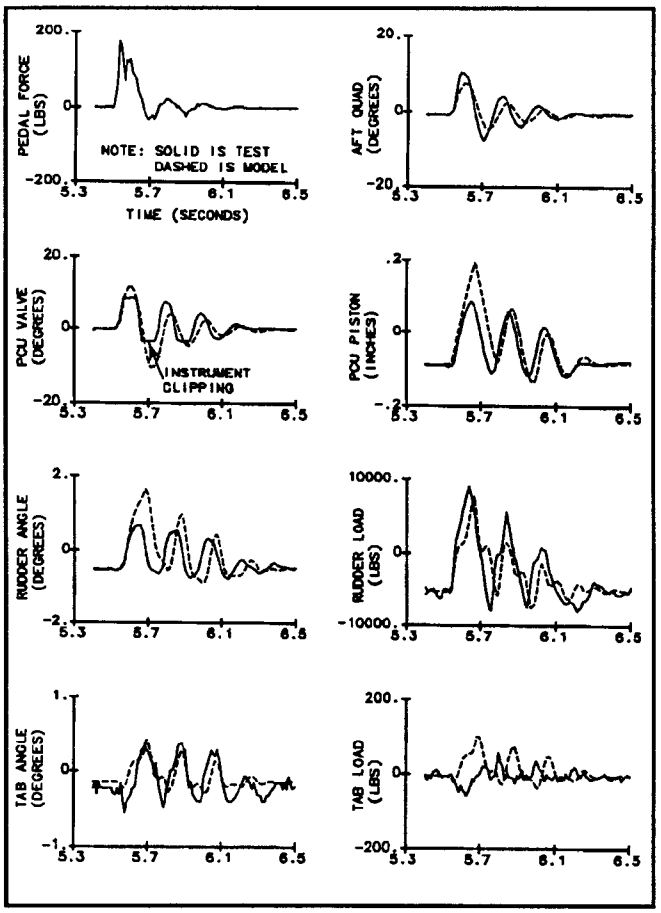

FIG. 16 Aero - Servo - Elastic Flutter Model Correlation To Successful April,16 1991 Flutter Test Data

During the investigation, limitations of linear analyses became obvious. Non-linear analyses, however, were impractical with large, complex models. Small, conceptual models were invaluable in understanding the non-linear behavior exhibited by the E-6 control system and fin structure. Extensive testing was required to identify and evaluate this behavior.

Solution of this challenging problem demonstrated that close cooperation and continuous communication among specialists from aerodynamics, flight controls, and structures are required to preserve a flutter free design.

Acknowledgements

This paper is dedicated to the memory of Steve Eng, Flight Controls Engineer - Boeing Defense & Space Group. Steve was a major contributor during the E-6 flutter investigation as well as being a friend and teacher to many. The authors of this paper thank the many individuals who participated in this investigation. Special thanks to: Boeing engineers Joe Bossi, Craig Campbell, Al Brown, Dean Clingman, Don Dorres, Glen Greisz, Bob Jones, John Morgan, Tony Olson, Henrik Straub, Al Swegle, and Dick

Williams; Boeing managers: Don Campbell, Paul Collins, John Hoos, Paul Stern, and Marv Walter; NAVAIR representatives: Hank Agnew, Pat Eng, and George Maggos; and Boeing consultant Dr. Holt Ashley of Stanford University for their assistance, encouragement and support of this effort. Special thanks to Scott Seagren for assistance in the preparation of this paper.

References

[1]Bendat, J., Enochson, L., and Piersol, G., *Analytical Study of Vibration Data Reduction Methods*, NASA CR55576, September 1963.

[2]Press, W., Flannery, B., Teukolsky, S.,Vetterling, W., *Numerical Recipes, The Art of Scientific Computing*, Cambridge University Press, 1986.

[3]Cannon, R., *Dynamics of Physical Systems*, McGraw-Hill Book Co., 1967.

[4]Hals, T., *Preliminary Results from Analytical Study on Stability Criteria for Hydraulic Servo Installations*, Boeing D6-58357-1, January 1968.

[5]MacNeal, R., *MSC / NASTRAN Handbook for Linear Analysis*, MacNeal Schwendler Co., August 1985.

[6]Gockel, M., *MSC / NASTRAN Handbook for Dynamic Analysis*, MacNeal Schwendler Co., June 1983.

[7]Guyan, R., *Reduction of Stiffness and Mass Matrices*, AIAA Journal, Vol. 3, No. 2, February 1965, pp 380.

[8]Gerald, C. and Wheatley, P., *Applied Numerical Analysis*, Addison-Wesley, 1984.

[9]Hammond, R., Harrison, J., and Kamber, P., *EASY5 Engineering Analysis System Reference Manual*, Boeing 20491-0503-R2, April 1989.